Design of Complex Semiconductor Integrated Structures

Cristina Arellano[*], Sergei Mingaleev, Andrey Novitsky[**], Igor Koltchanov[*], André Richter[*]**
[*]VPIsystems, Carnotstr. 6, 10587 Berlin, Germany. Phone:+49 30 398 058 30, Fax:+49 30 398 058 58
[**]VPI Development Center Minsk, Belarus
Cristina.Arellano@VPIsystems.com

Abstract: We present the benefits and limitations for designing complex optical semiconductor-based integrated structures by means of advanced numerical modeling. Multi-section tunable laser designs are presented and their tuning properties are analyzed for different architectures. We introduce a model of an integrated SOA with electro-absorption modulator. Its spectral properties are analyzed function of the parameters of the absorber section, showing the influence on the extinction ration of the generated signal. An InP-type Mach-Zehnder modulator is designed, illustrating the models of Kerr, Frank-Keldysh and QCSE effects. An example of a photo-detector demonstrates how dimensions and absorption parameters can be optimized to increase its detection bandwidth.

1. Introduction

Complex optical semiconductor-based integrated structures, also named Photonic Integrated Circuits (PICs), are increasingly gaining momentum, mainly due to their capability of integrating a large variety of complex multifunctional elements in a single device. Typical examples are multi-section lasers, tunable-laser modulators, SOA-MZI wavelength converters, and integrated optical phase-locked loops (OPLL) [1-2]. One of the main advantages of PICs is that they are compact sized implying fewer losses, and thus, less power consumption. Further on, they offer larger operation bandwidths compared to assembled circuits and are potentially low-cost devices as soon as a standardization fabrication process is available.

The variety of possible PIC architectures implies complexity in the modeling of such devices and their characteristics. Until recently, PICs were quite simple, combining only a few functional elements. They could be modeled either with home-made tools, or even analytically using plane-waves approximations and taking into account low communication speeds. With the increasing complexity, they include one or multiple highly nonlinear elements, which are difficult to model and account accurately for their interactions. Moreover, at low bit-rates, simple binary modulation formats or even a CW source were sufficient for understanding main properties of PICs. Now that the requirements of data signal transmission have been raised to 40-100 Gb/s, it becomes very important to model the PIC response to realistic driving signals, which may also be quite different for different modulation formats. Besides, commercial applications require estimation of the bit-error rate (BER) and other system performance measures, which are difficult to model without the help of professional Photonic Design Application (PDA) tools.

In the following section we will explain the generic model of the semiconductor cavity. Next, by means of illustrative examples, we will see how different types of semiconductor sections and effects can be modeled based on the transmission-line laser model.

All designs are created with *VPIcomponentMaker Active Photonics*.

2. Model of semiconductor cavities

Our model of the semiconductor cavity, denoted as Photonics-TLM, is an extension of the transmission-line laser model (TLLM) [3], which is based on the transmission-line matrix method (TLM) [4]. It is a time domain model, which supports the design of multi-section structures of bulk and multi-quantum well (MQW) medium.

The Photonics-TLM model divides the cavity into small, equidistant parts, named TLM-sections (Fig. 1). These TLM-sections are regarded as lumped scattering nodes interconnected by lossless transmission lines. Each scattering node represents the gain (stimulated emission), loss (scattering and absorption), noise (spontaneous emission) and grating-induced reflection that optical waves experience while passing through the section. The transmission lines connecting the scattering nodes of adjacent TLM sections represent waveguide propagation delays. The output optical fields from each scattering node are transferred to adjacent sections (back- and for-ward) every iteration.

Optoelectronic Materials and Devices IV, edited by Jian-Jun He, Guang-Hua Duan, Fumio Koyama, Ming C. Wu,
Proc. of SPIE-OSA-IEEE Asia Communications and Photonics, SPIE Vol. 7631, 76310K · © 2009 SPIE-OSA-IEEE
CCC code: 0277-786X/09/$18 · doi: 10.1117/12.852805

The final output of the Photonics-TLM is a stream of samples of the optical field separated by the defined time step. These samples are collected at the end of the cavity section. The optical spectrum can be calculated by Fourier transformation of the sample collection.

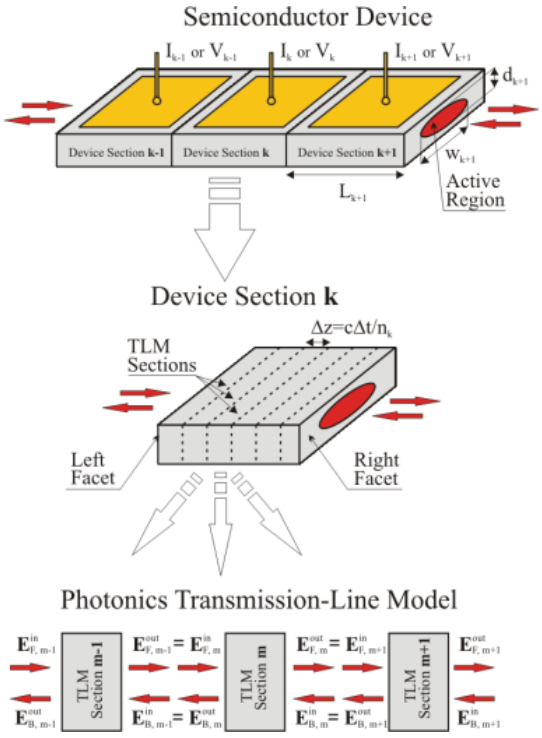

Fig. 1. Schematic of a semiconductor laser and the Photonics Transmission-Line Model (Photonics-TLM).

3. Application Cases

The Photonics-TLM model can represent four main types of device sections: passive, electro-optic, and active with linear or logarithmic gain model. Moreover, each device section may also contain a gain (loss) and index grating. This diversity allows simulating a large number of semiconductor devices such as lasers (ECL, DFB, FP), multi-section tunable lasers, optical amplifiers or electro-optical modulators.

To illustrate the statements above, we present in the following exemplary design cases of a multi-section tunable laser, an integrated semiconductor optical amplifier with reflective electro-absorption modulator (SOA-REAM), an InP-type Mach-Zehnder modulator (MZM) and a photo-detector. We will introduce the model for each device and analyze design and performance issues such as tunability, extinction ratio and modulation bandwidth.

3.1 Multi-section Tunable Laser

Wavelength-tunable lasers are key devices in WDM systems. They can be integrated, for instance, with an electro-absorption (EA) section [1] or in a more complex structure such as an OPLL [2]. In this exemplary case-study, we investigate a tunable distributed amplification (TDA) DFB laser, which served as basic mechanism of the device presented in [5]. We demonstrate how physical design parameters like the number and length of the laser sections influence the wavelength tunability and output power.

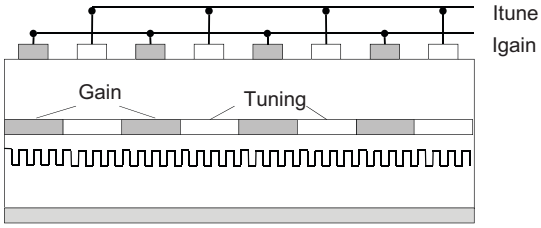

Fig. 2. Schematic of the TDA-DFB Laser.

The modeled device is represented in Fig. 2. The cavity contains a grating and is formed by alternate gain (SOA) and passive (tuning) sections. The active region type of the gain and tuning sections are MQW and bulk, respectively. One current contact is applied to each of the sections, where the injected current is divided for the gain and tuning sections, as shown in Fig. 2.

For passive sections, the electrical input signal models the bias current *Itune* which drives the carrier density dynamics in the active region, following the laser rate equation for carriers. In this case, the carrier dynamics in the electronic subsystem is considered to be independent of the photon carrier density. However, there is a reverse influence of the carrier density on the photon propagation due to the carrier-dependent internal loss and differential refractive index of the active region. In passive sections, spontaneous and stimulated light emissions are not considered.

In the gain sections, the carrier density dynamics in the electronic subsystem is assumed to be driven not only by the bias current, *Igain*, but also by spontaneous and stimulated emissions. The reverse influence of the carrier density on the photon propagation is determined not only by the carrier-dependent loss and differential refractive index of the active region, but also by the spontaneous light emission due to the bimolecular carrier recombination. The stimulated emission is described by the carrier-dependent and frequency-dependent gain profile. The frequency-dependent gain profile is approximated by a parabolic function with maximum at the gain peak. The parabola width and peak position are functions of the carrier density N. The peak gain grows linearly with N.

A grating is also included along the laser cavity. The grating is assumed to be made as corrugation of passive and gain sections. The corrugation provides loss, index and gain modulation depending on the loss indices and gains at either side of the corrugation. The strengths of the index and gain gratings are assumed to be carrier- dependent because of carrier-dependent changes in the refractive index and optical gain.

The device consists of a DFB cavity with 280 μm length. The length has been kept constant in all considered designs. The first design is formed by 8 sections that perform alternating gain and tuning functions. The length of the gain sections (*Lsoa*) is 40 μm, and 30 μm of the tuning sections (*Ltune*). In order to study the wavelength tunability and mode-hopping response of the laser, a continuous ramp current from 0 to 100 mA is applied to the tuning sections; the current of the SOA sections is swept in steps from 50 to 100 mA. The output frequency of the laser versus output power is displayed in Fig. 3, while Fig. 4 shows the output frequency versus the current injected into the tuning sections. It can be seen that mode-hop-free tuning is achieved in a range of about 400 GHz, which can allocate 8 ITU-channels with 50 GHz spacing. However, the output power of each channel has a variation of 5 dBm. A minimum current is necessary to start lasing, which corresponds to the output power where the frequency starts tuning (Fig. 3).

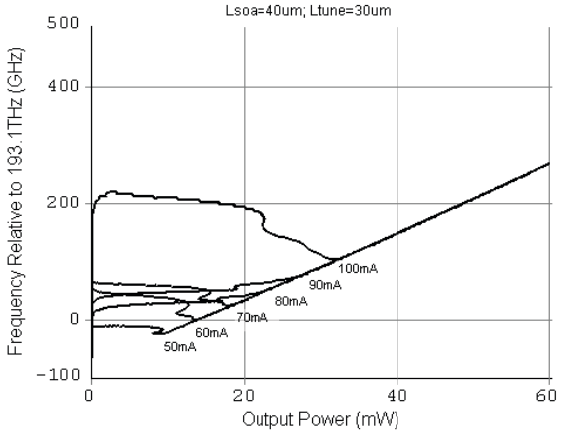

Fig. 3. Output frequency vs. output power for different values of SOA sections current. *Itune* ramps from 0 to 100 mA.

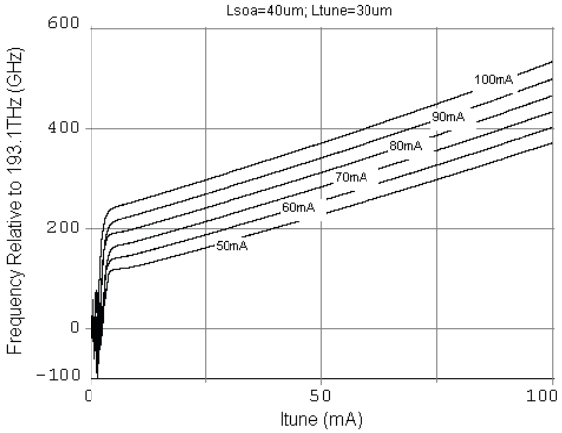

Fig. 4. Output frequency vs. input current at the tune sections for different values of SOA sections current.

In the following designs the length and number of the sections are varied while the total length of the device has been kept constant. Fig. 5 represents the results for lasers with 8 sections of different lengths. It can be seen that the laser presents mode-hopping when the SOA sections are shorter than the tuning ones. In Fig. 6, all sections have the same length, but the number of sections is varied. We observe that when increasing the number of sections, i.e. using sections with smaller length, the wavelength tunability and the output power increase. For the case of 4 sections or less, the laser shows mode-hopping.

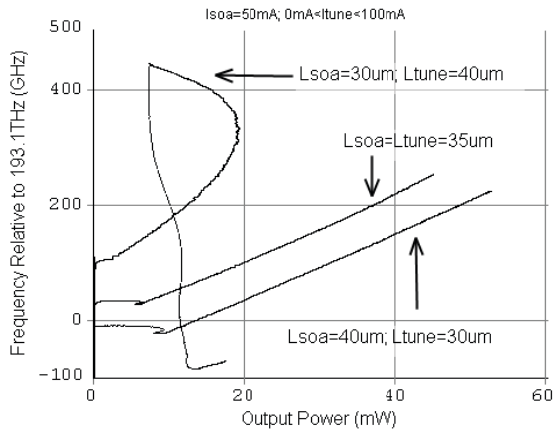

Fig. 5. Output frequency vs. output power for different values of section lengths.

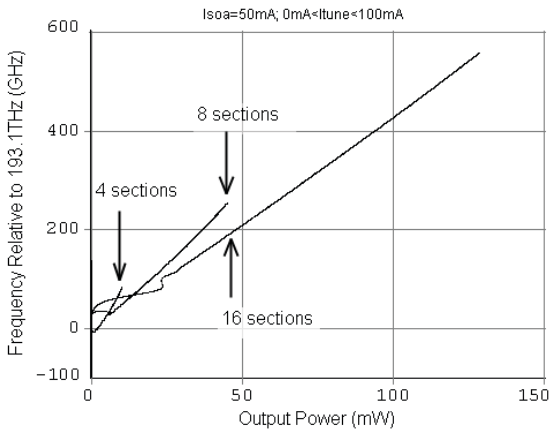

Fig. 6. Output frequency vs. output power at the tune sections for different number of sections.

3.2 Integrated SOA with Reflective Electro-Absorption Modulator

The use of a reflective SOA (RSOA) has been proposed several times to implement the Optical Network Unit (ONU) in WDM-PONs [6-8]. However, such elements have limited modulation bandwidth (2.5-5 Gb/s typically). An alternative is to use an integrated structure formed by an SOA section and an electro-absorber section [9], which can operate at higher bit rates of 10-40 Gb/s.

The EA modulator (EAM) model allows realistic modeling of the static and dynamic behavior of an EAM. In the EAM sections, the electrical input signal models a reverse-bias voltage which affects the refractive index and light absorption, due to the influence on the semiconductor band structure in the electronic subsystem. The refractive index changes linearly (Pockels effect) and quadratically (Kerr effect) with the applied voltage. Transitions in the valence-

conduction band cause the electro-absorption of light. Thus, depending on the type of the active region, it models either the quantum confined Stark effect (QCSE) or Franz-Keldysh effect (KFE). Such electro-absorption leads to the generation of carriers inside the active region, and accordingly induces a nontrivial carrier density dynamics in the electronic subsystem. This model also accounts for the frequency dependence on electro-absorption. The electro-absorption spectrum is approximated by a Lorentzian shape, which allows good accuracy for modeling of EAMs integrated with lasers and amplifiers. Similar to passive sections, in the EAM sections spontaneous and stimulated emission are not considered.

In this application example, the device is MQW-type, formed by one 200 μm long SOA-section with face reflection 10^{-12}, plus a 100 μm long EA-section with one high reflection (HR) face of 0.99. The SOA section is biased with a fixed current of 100 μA; the data signal is applied at the EA section with bias voltage swinging between -5 V (spaces) and 0 V (marks).

Due to the properties of electro-absorption, the spectral response of the device strongly depends on the applied voltage. As a result, each ONU would transmit with a different power level and signal quality (Fig. 7). The spectral properties of EA can be adjusted in order to homogenize the different WDM channels by adjusting the voltage dependency of the peak absorption (f_{abs}) and absorption bandwidth (BW_{abs}) (Fig. 8).

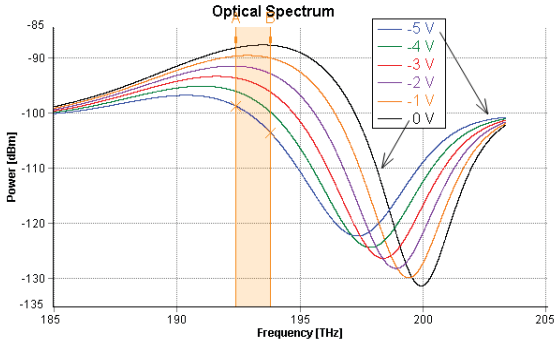

Fig. 7 Output spectra of the SOA-REAM for f_{abs}=0.5 10^{12} Hz/V and BW_{abs}=-0.6 10^{12} Hz/V.

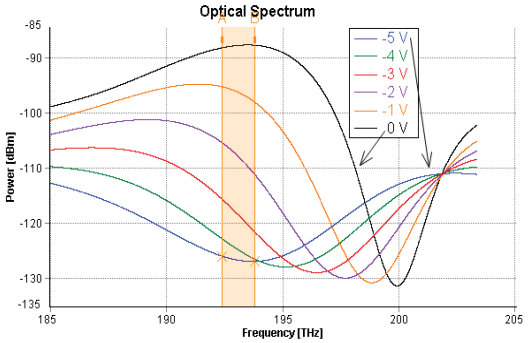

Fig. 8 Output spectra of the SOA-REAM for f_{abs}=10^{12} Hz/V and BW_{abs}=-2.5 10^{12} Hz/V.

Fig. 9 shows the eye diagrams for the channels at 192.4 THz and 193.8 THz, representing the outer channels of a 16 channel 100GHz-spaced WDM band. The extinction ratio is in the order of 30 dB. The difference in the mark levels of the two extreme channels is approximately 1.5 dB.

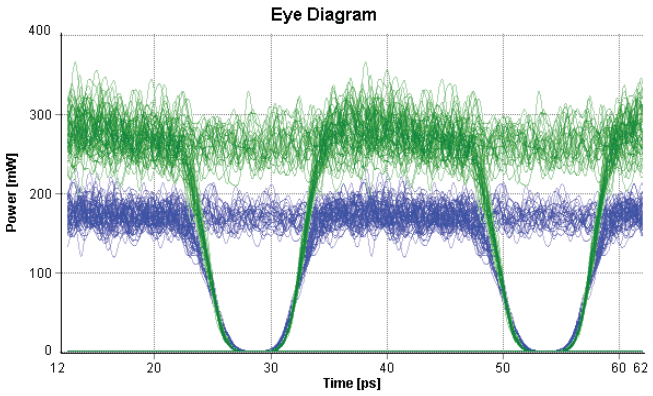

Fig. 9 Eye diagrams at 40 Gb/s for channels at 192.4 THz (blue) and 193.8 THz (green).

3.3 InP-type Mach-Zehnder Modulator

In the previous section we have discussed an example of a direct modulated device capable of operating at 40 Gb/s. However, external Mach-Zehnder based modulators (MZM) are still preferred for high speed applications (40 Gb/s or more) and complex modulation formats.

Traditionally, MZMs are built on $LiNbO_3$. Such modulators are based on the Pockels effect, which represents the linear change of the refractive index with the applied bias voltage (see application that is described in section 3.1). Besides $LiNbO_3$ modulators, the progress in monolithic integration is growing the development of InP-based integrated transmitters, with the benefits of lower voltage drive requirements, shorter devices and availability of integration with laser sources or optical amplifiers. InP modulators are based on the Kerr and Frank-Keldysh effect (bulk) or QCSE (MQW) so that the refractive index change is quadratic with voltage and the absorption change is linear with voltage [10]. The electro-refractive effect enables to build MZMs with low voltage drive requirements (2-3 V) and with electrode lengths around 1 mm. Such devices can be modeled using EAM sections, as described in section 3.2.

The Photonics-TLM uses phenomenological modeling of electro-refraction effects assuming that the change of the group effective index of the guided optical mode is described as a sum of terms:

$$\Delta n = r_1 V + r_2 V^2 + \frac{dn}{dN}(N - N_0)$$

The first two terms represent the electro-refractive index change that occurs in electro-absorption sections. It may be caused by the Pockels and Kerr effects and are described by the linear (r_1) and quadratic (r_2) change of refractive index with voltage (V). The last term represents the carrier-dependent refractive index change, which occurs in all device sections. Here, dn/dN is the differential refractive index, N is the carrier density and N_0 is the chirp-reference carrier density for which the chirp-induced frequency offset is zero.

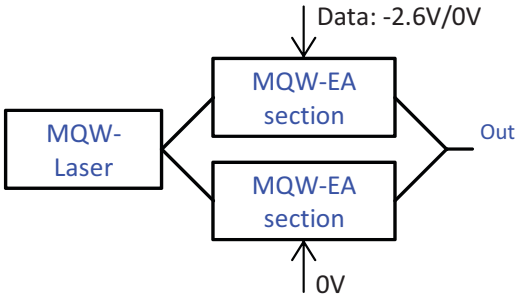

Fig. 10 Schematic of the Mach-Zehnder transmitter.

As an example we present the model of an InP-MZM based on MQW-EA sections. The modulator follows the structure represented in Fig. 10. The length of the EA sections is set to a typical value of 1.1 mm [11]. The laser is a DFB-type with MQW structure, 300 μm long. The bias voltage is swept to determine the phase change, which is directly related to the refractive index change by

$$\Delta\phi = \frac{2\Pi\Delta nL}{\lambda}$$

with Δn the refractive index change and L the section length. Here, the voltage for which the phase increases $\prod$ radian is found to be 2.6 V (Fig. 11), which corresponds with a typical value for a device with these physical parameters. From here, the modulator can be extended to more complex integrated structures, such as I-Q transmitters, and optimized by varying the different physical parameters of the design, such as length or linear and quadratic refractive coefficients, for instance.

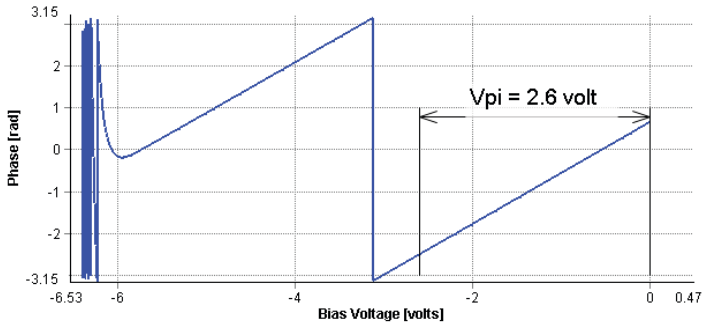

Fig 11. Phase of the transmitter output signal function of the applied bias voltage.

3.4 Photo-detector with an Electro-Absorption section

The Photonics-TLM model outputs all variables that are observable in real systems, among them not only the intensity waveforms and optical spectra, but also the junction voltage and photocurrent that take place in the electrical terminal. Specifically for EA sections, the photocurrent that is output of the model is described as:

$$I = \frac{q\ vol}{n\_sec} \sum_{m}^{n\_sec} \frac{N_m}{\tau_0(N_m)}$$

where q is the electron charge, *vol* is the volume of the active region, *n_sec* is the number of TLM-sections, N_m is the carrier density within a TLM-section, and τ_0 is the carrier-dependent sweep-out constant. Electrons swept out from the active region to the output contacts generate the photocurrent. Hence, photo-detectors can also be represented by means of the EA model, choosing the adequate parameters. For exemplification, we design a waveguide-integrated PIN photodiode [12]. The device consists of a EA section with dimensions of 20 μm length, 5 μm width and 0.4 μm absorption region thickness.

By adapting the sweep-out constant, the detection bandwidth can be significantly improved as depicted in Fig. 12, which shows eye diagrams of a 100 Gb/s-modulated signal after detection. In this example, the optical input power in 1 mW. By observing Fig. 12, the resistivity is found to be 0.6 A/W for a reverse bias voltage of 1 V.

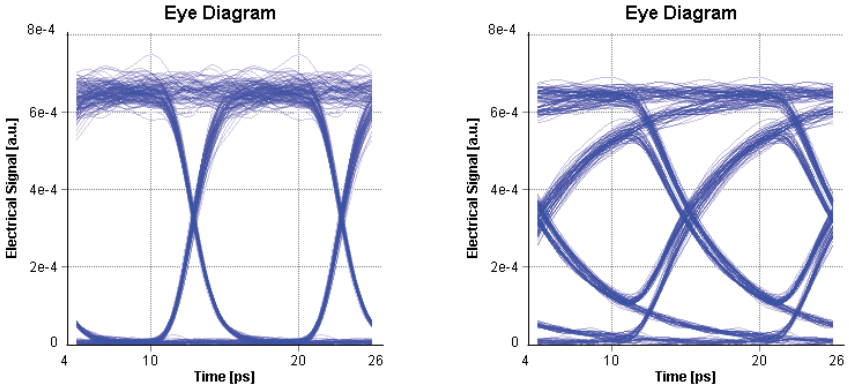

Fig. 12 Eye diagrams of a 100 Gb/s-modulated signal after detection with the EA model for sweep-out constants of 1 ps (left) and 5 ps (right). Bias=-1 V.

4. Summary

We presented important aspects of the design of complex semiconductor integrated devices and showed a method for modeling active, passive and absorption devices with different types of active region and the possibility of combining them. We demonstrated that the flexible Photonics-TLM model – integral part of *VPIcomponentMaker Active Photonics* – is well suited to address those photonic integrated circuit applications. We discussed several exemplary design studies covering a large diversity of components: a multi-section tunable laser, an integrated SOA with electro-absorption modulator, a InP-type Mach-Zehnder modulator and a photo-detector.

Acknowledgement

This work has been partly supported by the Federal Ministry of Education and Research, Germany in framework of the European Celtic project 100GET.

References

[1] S. Sekiguchi, K. Takabayashi, A. Hayakawa, S. Tomabechi, A. Uetake, M. Ekawa, and H. Kuwatsuka, "10 Gb/s Wavelength-Tunable EML with Continuous Wavelength Tuning Covering 50 GHz x 8 Channels on ITU Grid", in proc. OFC/NFOEC 2007, OMS4.

[2] S. Ristic, A. Bhardwaj, M.J. Rodwell, L.A. Coldren, L.A. Johansson, "Integrated Optical Phase-Locked Loop", in proc. OFC/NFOEC 2009, PDPB3.

[3] A.J. Lowery, "A new dynamic semiconductor laser model based on the transmission line modeling method", IEE Proc. J. Optoelectron., Vol. 134 (5), Oct. 1987.

[4] W.F. Hoefer, "The Transmission-Line Matrix Method – Theory and Applications", IEEE Trans. on Microwave Theory and Techniques, Vol. MTT-33 (10), Oct. 1985.

[5] H. Ishii, Y. Kondo, F. Kano, and Y. Yoshikuni, "A Tunable Distributed Amplification DFB Laser Diode (TDA-DFB-LD)", IEEE PTL Vol. 10 (1), Jan. 1998.

[6] J. Prat, C. Arellano, V. Polo and C. Bock, "Optical network unit based on a bidirectional reflective semiconductor optical amplifier for fiber-to-the-home networks", IEEE PTL, Vol. 17 (1), Jan. 2005.

[7] F. Payoux, P. Chanclou, T. Soret, N. Genay and R. Brenot, "Demonstration of a RSOA-based Wavelength Remodulation in 1.25 Gbit/s Bidirectional Hybrid WDM-TDM PON", in proc. OFC/NFOFC 2006, paper OTuC4.

[8] M. Omella, I. Papagiannakis, B. Schrenk, D. Klonidis, J.A. Lázaro, A.N. Birbas, J. Kikidis, J., and I. Tomkos, "10 Gb/s full-duplex bidirectional transmission with RSOA-based ONU using detuned optical filtering and decision feedback equalization", Optics Express, Vol. 17 (7), March 2009.

[9] A.Garreau, J.Decobert , C. Kazmierski, M-C. Cuisin, J-G. Provost, H.Sillard, F.Blache, D.Carpentier, J.Landreau and P.Chanclou, "10Gbit/s Amplified Reflective Electroabsorption Modulator for Colourless Access Networks", in proc. IPRM 2006, paper TuA2.3.

[10]J. G. Mendoza-Alvarez, L. A. Coldren, A. Alping, R. H. Yan, T. Hausken, K. Lee and K. Pedrottin, "Analysis of Depletion Edge Translation Lightwave Modulators", IEEE JLT, Vol. 6 (6), Jun. 1988.

[11]R.A. Griffin, "Advanced Optical Modulators on InP", in proc. LEOS 2007, ThX1.

[12]A. Beling, 'InP-Based High-Speed Photonic Devices', in proc. OFC/NFOEC 2008, OMS2.